Transient three-dimensional simulation of a metal hydride hydrogen storage tank interconnected to a PEM fuel cell by heat pipes

Farshid Mahmoodi[1], Rahbar Rahimi[2*]

[1] PhD student, Department of Chemical Engineering, Faculty of Engineering, University of Sistan and Baluchestan, Zahedan, Iran.
[2] Department of Chemical Engineering, University of Sistan and Baluchestan, Zahedan, P.O. Box 98164-161, Iran.

Abstract

PEMFC heat generation was utilized to desorb hydrogen from a $LaNi_5$ filled MH–Hydrogen Storage tank. Heat pipes were used to transfer heat from the FC to the MH- tank. The study was conducted using CFD simulation. Results showed that the increase of initial pressure of the MH tank and the cooling temperature of 303 K led to a rise in the hydrogen adsorption performance.After 4000 s in the desorption stage, 5.39 g of hydrogen was purged from the hydride tank. Additionally, results demonstrated that a total hydrogen discharge rate of 0.304 slpm was achieved only at the expense of 7.36 W of the total 23.43 W generated heat in the fuel cell. Furthermore, the hydrogen desorption flow rate gained 45% for the presented geometry compared to a similar system. Moreover, a very good agreement was found between the present work simulation results and the literature data.

1. Introduction

Since fossil fuels have caused considerable environmental problems, hydrogen, as the cleanest renewable energy carrier, is expected to quickly replace fossil fuels in the future [1, 2]. In particular, one possible use of hydrogen is to provide the electrical power required for various devices through

the Proton exchange membrane fuel cell (PEMFC), which will reduce environmental pollution. The use of hydrogen as fuel in vehicles is divided into three types: (1) in a nickel-hydride battery, in which hydrogen is combined as an MH, (2) in vehicles with a sparkle ignition engine, and (3) in the fuel cell [3]. PEMFC is a system in which fuel (mostly hydrogen) and oxygen electrochemically react and generate electricity, heat, and water. The efficiency of a PEMFC in generating electricity is relatively high (up to 55%), but a significant amount of heat is produced as a by-product, which should be effectively removed to maintain the fuel cell's temperature in its optimal range. PEMFC typically operates at relatively low temperatures (60 to 80 °C), which allows this type of fuel cell to be considered a proper option for various static and dynamic applications where a quick set-up is needed   with appropriate efficiency and environmentally clean electricity [4,5]. The heat produced during PEMFC operation can be exploited and utilized in many heating applications such as hot water supply, heating of different spaces, and heating of various reactants in cold air conditions [6, 7].

In many usages, a metal hydride (MH) hydrogen storage system is used to supply hydrogen for the PEMFC [5, 8]. The heating of the MH storage system and its operation at temperatures above the typical ambient temperature can significantly increase the rate of hydrogen release from the MH storage system. By applying heat pipes, the heat generated in the fuel cell can be effectively transferred to MH storage systems [9, 10]. Heat pipes have high thermal conductivity and can carry most of the heat generated in the fuel cell into an MH storage system without needing extra power to pump it. Another advantage of heat pipes are their simplicity of structure and lower maintenance costs due to the lack of moving components in their structure; moreover, the heat pipes can also provide an excellent temperature control mechanism compared to many other passive cooling methods [11].   Heat pipes operation is based on the specified equilibrium pressure and liquid boiling point assigned to the heat pipe. Previous research has demonstrated that it is impossible to use the full hydrogen storage capacity of the MH system in a the thermal coupling an MH storage system and a PEMFC stack using a water circuit without heat coupling [12]. Furthermore, increasing the effective length of the heat pipe and reducing the heat pipe diameter would reduce the ability of stack cooling [5]. In another work, a study of stirring effect on the hydrogen adsorption in an MH tank indicated that stirring increased the hydrogen uptake [13]. The use of a spiral coil heat exchanger in hydrogen removal from a magnesium hydride reactor improves the mass and heat transfer of the reactor [14]. During hydrogen injection, the MH porosity decreases, but the porosity increases along with hydrogen depletion [15]. Saleh et al. [16], develop a model which can be extrapolated to higher wattage fuel cells. They tried to determine the effect of air compared to oxygen in a full cell by only simulating the fuel cell with a zero-dimensional model to investigate the wattage, the effect of electric and thermodynamic variables, and different operational conditions. Unfortunately, they do not report their results. Other studies have shown that the use of an effective thermal coupling, such as PEMFC heat exchangers, and a hydrogen MH storage system is essential to improve thermal management, thereby increasing the efficiency of fuel cells [17].

In this project, the thermal coupling of PEMFC with an MH hydrogen storage tank using heat pipes was studied by means of mathematical modelling and numerical simulation. In this work, the designed system was numerically analyzed based on the Navier Stokes equation as well as mass and energy equations. Computational fluid dynamics (CFD) was used to solve the model equations. The system is designed so that in the first stage, hydrogen is adsorbed in the hydride reservoir. In the second stage, part of this hydrogen is released for use in a PEMFC. There are few works in the literature about the thermal coupling of PEM fuel cell to a metal hydride storage tank using heat pipes. In fact, most of the previous works have only estimated the output voltage of fuel cell under various conditions [12, 16, 23]. The present work precisely investigates the H_2 adsorption and desorption

progress in detail. It also analyzes the subsequent effect of an increase in the number of heat pipes during thermal coupling. This study introduces a new geometric configuration for the thermal assistance of PEM fuel cell for H_2 desorption from a metal hydride storage tank using heat pipes. in this configuration the heat released in the cathode channel of the fuel cell is directed to the MH storage, and hydrogen is released at a higher rate. Also, in the presented geometry, the condenser part is located inside the MH tank which is a new design compared to other studies [5, 18]. Lastly, the dependence of the generated heat in the fuel cell and the heat required in the MH tank have been studied by hydrogen release and consumption.

2. System Geometry

In the mathematical modelling of the study system, the main considered assumptions are:

- A three-dimensional unsteady-state model was applied to the entire system.
- The production of water in the PEMFC was considered to be in the form of steam in the operating temperature range.
- Hydrogen and oxygen were considered as an ideal gas in the operating range of PEMFC.
- The amount of work due to hydrogen compression and the amount of energy loss due to the viscosity effects.
- The amount of radiate heat transfer was considered insignificant.
- MH reservoirs were fully insulated and their thermal loss to the atmosphere was considered insignificant.
- The uniformity of solid MH and hydrogen gas temperatures due to thermal equilibrium was assumed.
- The dependency of hydrogen equilibrium pressure to its concentration was considered insignificant.
- The fluidity of the heat pipe fluid was considered as a Newtonian fluid as well as the laminar flow of this fluid through the heat pipe.
- The pressure drop of fluid flow inside the wick

structure of the heat pipe was calculated by the Darcy equation.
- The isolation of the adiabatic part of the heat pipe was assumed, and the heat loss in the condensation region and the evaporation regions of the heat pipe were considered insignificant.

As illustrated in Fig. 1, the system consists of a storage tank, heat pipes, cathode, gas diffusion layer (GDL), electrode, membrane, anode, and cooling water tube. In the design of this system, it is assumed that the bodies of the heat pipes, cooling water tube, and storage tank are made of copper metal. Also, with regard to other scientific sources, the metal powder in the storage tank is made of $LaNi_5$. In the first step, it is assumed that there is only one hydrogen storage system.

Therefore, at this stage, a certain amount of hydrogen with a concentration of y_{H2} from the top of the reservoir enters the reservoir at a constant pressure P, and then it is assumed that the input is closed and the bed remains for the duration of t in the same conditions until the hydrogen is adsorbed over the metal powder over time. Since the hydrogen adsorption process is a heat-exothermic process, a low-temperature cooling water stream is embedded throughout the inside of the chamber to remove heat generated by this process. At this stage, this heat depletion will help to increase the amount of hydrogen adsorption on the metal powder. Once the hydrogen adsorption has been completed, it is time to use the adsorbed hydrogen in the fuel cell. During the desorption operation, hydrogen is removed from the top of the reservoir and directed to the entrance of the fuel cell anode channel. Hydrogen, which may contain some water vapour, enters the anode (where the only hydrogen present is from the inside of the GDL) and penetrates through the membrane into the cathode channel, whereby it reacts with the oxygen that enters the cathode and produces electricity and some heat. Each heat pipe consists of three sections: evaporator, adiabatic, and condenser. The evaporator part is located entirely in the cathode channel and all parts of the condenser portion are located in the hydrogen storage chamber. The role of each of the
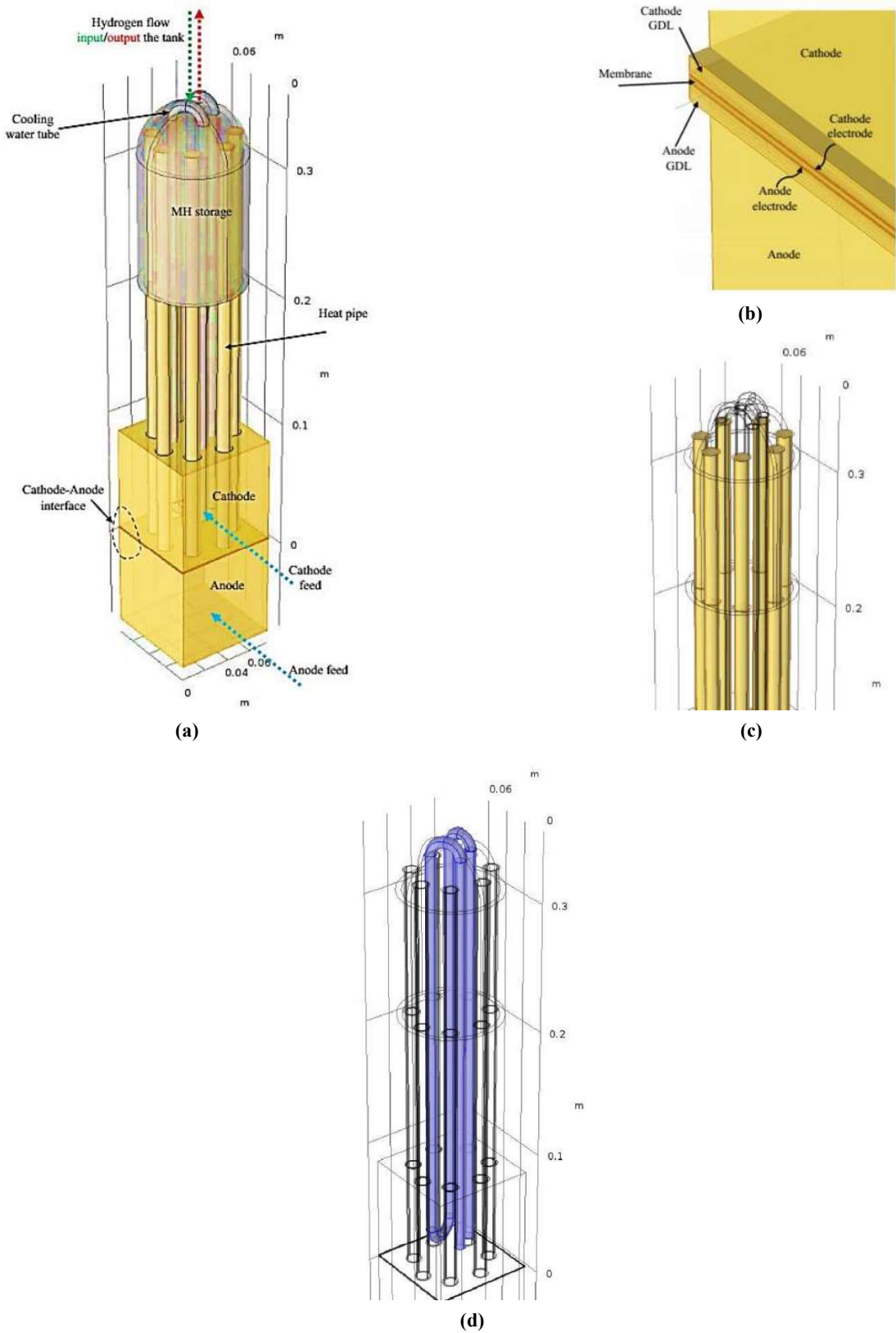
(a)

(b)

(c)

(d)

Fig. 1. a) The overall schematic of the system (geometrical plan studied in this work), b) The schematic of the gas diffusion layers and membrane, c) The schematic of the heat pipes, d) The schematic of the cooling water tube.

heat pipes is to direct the heat released in the cathode channel to the storage chamber and help to release hydrogen at a higher rate, due to the endothermic process of the operation of hydrogen removal from the hydride bed. In Table (1), the physical parameters of each part of the system are presented.

It is worth noting that water is used as the working fluid in all heat pipes in the simulations. In the cathode, available water in the evaporator part receives heat from the generated heat and is converted to steam. The steam passing through the adiabatic part neither loses nor receive heat, it then enters the condenser section where some heat is transferred to the reservoir due to the lower temperature of the hydride reservoir, causing its temperature to drop. In this case, the steam is condensed and drops through the walls of the heat pipe. In the designed system, the heat pipes can be easily be separated from the MH tank after discharge.

These heat absorption and desorption cycles provided by the working fluid of the heat pipe continue until the end of the process. The physical values of thermal and mass penetration are summarized in Table 2.

The heat and mass transfer in the MH tank is specified by bellow equations below [5, 19, 20]:

$$\left(\rho C_p\right)_{eff}\frac{\partial T_{MH}}{\partial t}+\rho C_p U.\nabla T_{MH}+\nabla.q = Q+Q_p+Q_{vd} \tag{1}$$

On left-hand side of Eq. 1, the first, second and third terms are related to energy accumulation, convection heat transfer, and conduction heat transfer, respectively.

$$q = -k_{eff}\nabla T_{MH} \tag{2}$$

$$\left(\rho C_p\right)_{eff} = \theta_p \rho_p C_{pp} +\left(1-\theta_p\right)\rho C_p \tag{3}$$

Table 1. Physical parameters of the system geometric used in the simulations.

Parameter	Value (mm)	Parameter	Value (mm)
dtank	75	dhp	6
Ltank	132	δhp	0.85
δtank	4	δwick	0.356
dwt	12	Lcell	75
Lev	80	Lchanel	80
Lad	125	wchanel	75
Lcon	110	wGDL	0.380
δelec	0.05	δmem	0.1

Table 2. Parameters for mass and heat transfer [15, 20]

Parameter	Value	Parameter	Value	Parameter	Value
ε_{GDL}	0.4	Cp_{O2} (j/kg.K)	919	M_{metal} (g/mol)	432
k_{GDL} (m²)	1.18×10^{-11}	Cp_{steam} (j/kg.K)	1970	ω_{ads} (s⁻¹)	10
Ω_{GDL} (S/m)	222	Cp_{H2} (j/kg.K)	14.89	ω_{des} (s⁻¹)	15
μ_a (Pa.s)	1.19×10^{-5}	Cp_{metal} (j/kg.K)	419	E_{ads} (j/mol)	27200
μ_c (Pa.s)	2.46×10^{-5}	μ_{H2} (Pa.s)	8.411×10^{-6}	E_{des} (j/mol)	23468
$D_{H2\text{-}H2O}$ (m²/s)	1.8×10^{-4}	ε_t	0.5	ΔH (j/mol)	29879
$D_{N2\text{-}H2O}$ (m²/s)	5.05×10^{-5}	k_t (m²)	1×10^{-8}	ΔS (j/mol)	108
$D_{O2\text{-}N2}$ (m²/s)	4.7×10^{-5}	K_{H2} (W/m.K)	0.1672	h (W/m².K)	10
$D_{O2\text{-}H2O}$ (m²/s)	5.53×10^{-5}	K_{metal} (W/m.K)	3.18	Weight of metal powder (g)	232
ν_m	0.3	K_{water} (W/m.K)	0.61	ρ_{empty} (kg/m³)	4200
Ω_m (S/m)	9.825	K_{O2} (W/m.K)	33.7×10^{-3}	ρ_{sat} (kg/m³)	4226
C_{O2} (j/kg.K)	259.8	K_{copper} (W/m.K)	400	C_a	2
C_{steam} (j/kg.K)	461.52	K_{steam} (W/m.K)	0.0188	C_d	1

$$k_{eff} = \theta_p k_p + \left(1 - \theta_p\right)k + k_{disp} \tag{4}$$

$$\varepsilon_p \rho \frac{\partial w_i}{\partial t} + \nabla J_i = R_i \tag{5}$$

On left-hand side of Eq. 5, the first and second terms are related to mass accumulation and mass diffusion, and the right-hand side term represents reaction.

$$J_i = -(\rho w_i \sum_k D_{e,ik} d_k + D_{e,i}^{\ T} \frac{\nabla T}{T}); Maxwell-Stefan \tag{6}$$

Eq. 6 is the Maxwell-Stefan relation which describe the diffusion model in multicomponent systems.

$$D_{e,ik} = \frac{\varepsilon}{\tau_F} \cdot \left(\frac{1}{D_{ij}} + \frac{1}{D_{ik}}\right)^{-1} \tag{7}$$

$$d_k = \nabla_{x_k} + \frac{1}{p_A}\left[\left(x_k - w_k\right)\nabla_{PA}\right] \tag{8}$$

$$x_k = \frac{w_k}{M_k} M_n \tag{9}$$

$$r_{MV,i}^{for} = k^f \prod \left(\frac{\rho w_r}{M_r}\right)^{-v_i,r} \tag{10}$$

$$r_{MV,i}^{rev} = k^r \prod(\frac{\rho w_p}{M_p})^{-v_i,p} \tag{11}$$

Where,
Adsorption step

$$q_{0,1} = h\left(T_{MH} - T_{ext}\right)|_{tank\ wall} \tag{12}$$
convection with surrounding

$$q_{0,2} = h\left(T_{MH} - T_{water\ wall}\right)|_{water\ tube\ wall} \tag{13}$$
convection with the cooling tube wall

$$q_{0,3} = k\frac{\partial T}{\partial x}|_{water\ tube\ wall} \tag{14}$$
conduction with the cooling tube wall

$$R_i = v_i M_i r_{MV,i}^{for} - r_{MV,i}^{rev} \tag{15}$$

$$-nJ_i|_{tank\ wall} = 0 \tag{16}$$
no mass flux on the tank wall

Desorption step

$$-nq_{tank\ wall} = 0 \tag{17}$$
diabatic wall

$$q_0 = k\frac{\partial T}{\partial x}|_{heat\ pipe\ wall} \tag{18}$$
conduction with heat pipe wall

$$q_0 = h\left(T_{heat\ pipe} - T_{MH}\right)|_{tank\ wall} \tag{19}$$
convection with heat pipe wall

$$-n.\rho\omega_i \sum D_{ik}d_k|_{tank\ output} = 0 \tag{20}$$
output H_2 flow from the tank

It is worth noting that the initial conditions for adsorption and desorption are shown in Table 3.

Table 3. Initial condition for adsorption and desorption.

Initial conditions	Adsorption	Desorption
Hydrogen (gr)	0	Adsorbed hydrogen from the latest desorption step
Temperature	25°C	Temperature of the latest desorption step

The reaction of hydrogen atoms with metal alloys to form MHs is as follows:

$$M_e + \frac{x}{2}H_2 \leftrightarrow M_e H_x + Q_{react} \tag{21}$$

Where M_e is the metal or alloy materials, H is a hydrogen atom, $M_e H_x$ is a metal hydride, x is the ratio of hydrogen atoms to metal or alloy, and Q_{react} is the heat released or absorbed during the process of hydrogen adsorption and desorption [5].

The kinetic equation of the hydrogen adsorption reaction in the MH system is given below by assuming that the thermal equilibrium between hydrogen and the MH alloy of the energy equation is true [21]:

$$\frac{dx}{dt} = C_a e^{\left(\frac{-E_a}{RT}\right)\left(\frac{P_{H_2} - P_{a_{eq}}}{P_{a_{eq}}}\right)}\left(X_{max} - X\right) \tag{22}$$

In which, according to weight percentage (wt%), X and X_{max} are the amounts of adsorbed hydrogen and the maximum amount of adsorbed hydrogen,

respectively.

The kinetic equation of the hydrogen desorption process is as follows:

$$\frac{dx}{dt} = C_d e^{\left(\frac{-E_d}{RT}\right)\left(\frac{P_{H2-}P_{d_{eq}}}{P_{d_{eq}}}\right)} X \tag{23}$$

Where R is the global constant of gases, T is the temperature of the bed, P_{H2} is the hydrogen pressure, and $P_{a,eq}$ and $P_{d,eq}$ are the equilibrium pressure of hydrogen adsorbed and desorbed, respectively.

The equilibrium pressure P_{eq} is determined by the below equation as a function of temperature [20]:

$$\frac{P_{eq}}{P_{ref}} = 10^{-5} e^{\left(\frac{-\ddot{A}H}{RT} + \frac{\ddot{A}S}{R}\right)} \tag{24}$$

Where ΔH and ΔS are enthalpy and entropy of reaction of hydrogen with metal alloys according to Eq. 21, as shown in Table 2. Also, the relations for calculating capillary pressure in the heat pipes were adopted from the literature [5].

In the solution procedure, three elements sizes were investigated for the study of mesh independence, the coarse mesh with an element size of 11.9 mm, normal mesh with an element size of 7.67 mm, and the fine mesh with an element size of 4.26 mm.

3. Results and discussion

In this research, the CFD calculation of Navier Stokes equation and mass and Energy conservation equations were carried out using the finite element method (FEM) in COMSOL Multiphysics® Modeling Software 5.3a. The multi-frontal massively parallel sparse direct (MUMPS) algorithm was used in COMSOL. This is a nonlinear equation solving method in which the set of nonlinear equations are first transformed into a system of linear equations and then solved in parallel. This method is typically part of Gaussian elimination methods, unlike in other systems of linear equations similar to this study, where discretization is performed by the finite element method (FEM). Using the user controls, the

edge values of the studied geometry were manually defined in COMSOL so that the entire geometry could be meshed. The reason for using user control is to do the meshing quickly to decrease the number of required equations. Two form can be considered for convergence in the finite element method: number of iteration and minimum pointwise deviation (δ). In this research a minimum pointwise deviation of δ=10⁻³ was used.

When solving the fuel cell stack models using CFD simulation, one should carefully mesh the geometry in order to reduce the number of degrees of freedom (DOF) without affecting the simulation results. Mesh independency tests must be performed for the fuel cell models. Three mesh sizes can be considered: normal mesh, fine mesh and coarse mesh. Fig. 2 shows a mesh independency test for hydrogen flow rate. As can be seen from this figure, using the normal size of mesh obtained results almost the same as the solution values corresponding to that of fine size unlike the results of the coarse size mesh, which are is quite different from the other two. Since normal mesh size can be used for the faster run time, it was used in this study.
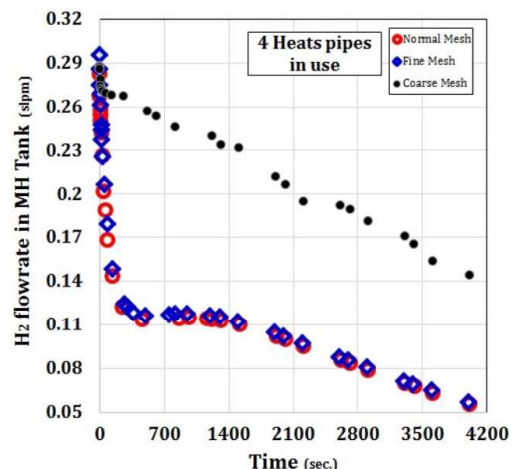

Fig. 2. Mesh independency test for hydrogen flow rate from the MH tank as a function of time.

Fig. 3 shows the profile of the adsorbed hydrogen on the metal powder in the adsorption stage. At the beginning of the adsorption operation, the metal powder is free of hydrogen, and the mass transfer driving force (the difference in the hydrogen concentration in the
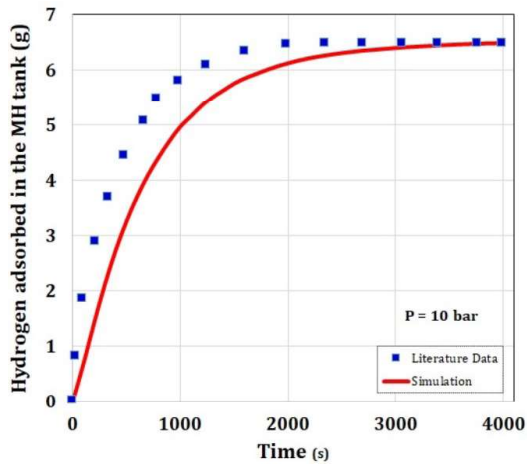
Fig. 3. Hydrogen adsorption over time and compared with literature data [13, 20].

Fig. 4. Temperature changes of the adsorption bed over time at 10 bar compared with literature data [22].

gas phase and solid phase) is in its maximum state. Therefore, based on the rule, it is expected that after the initial times the hydrogen adsorption will experience a sharp increase in the slope.

Over time, when the mass transfer driving force decreases due to the adsorption of hydrogen on the metal powder, the amount of adsorbed hydrogen is constant and the concentration gradient will be close to zero. This figure shows the changes in the amount of adsorbed hydrogen compared with the data of a scientific source [5] and that the simulation results in this work are consistent with the literature data. Also, the results of this figure indicate that the MH reservoir can store the amount of 7.5 gr of hydrogen in the reference conditions. In Fig. 4, the temperature changes of the hydrogen adsorption bed are plotted at a pressure of bar 10 over time. As mentioned in the interpretation of Fig. 3, at the initial moments of the process the mass transfer driving force has its maximal value, and therefore, in this case, a sharp incremental slope in temperature change is to be expected.

The hydrogen adsorption operation is an exothermic process. Therefore, during the adsorption operation, a certain amount of heat is released (as much as the heat of the adsorbed hydrogen onto the metal). Fig. 4 shows that the temperature of the adsorption bed increases from 293.15 K to about 335.15 K in only 80 seconds because of the heat released at the beginning of the adsorption operation. Since heat is released so
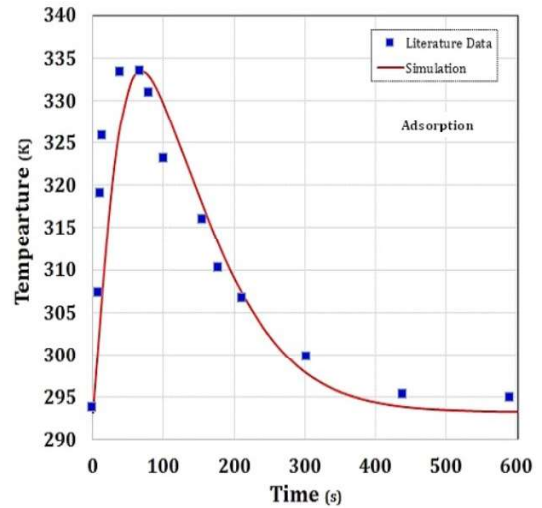
earlydue to the high mass transfer driving force, the cooling water flow is not able to transfer the reservoir heat out and reduce its temperature. Thus, at first the temperature of the bed increases, and then over time the temperature of the reservoir decreases to an equilibrium constant value (similar to the initial temperature) due to the reduction of the mass transfer driving force, the reduction of released heat during the adsorption operation, and as the cooling water performance increases. Also, in this figure, the simulation results were compared with the literature data [22], and showed very good agreement and high simulation accuracy. Changes in the temperature of the hydride bed during the desorption operation are shown in Fig. 5. Due to the separation of hydrogen from the metal powder, some constant heat is used to disport the hydrogen molecules from the metal powder ones during the hydrogen desorption operation from the hydride bed. The desorption operation is inherently endothermic and is therefore expected to reduce the temperature of the system based on the rule.

As seen in Fig. 5, the temperature of the system decreases from 323.15 to 278.15 K from the beginning to about 30 seconds after the desorption operation. Since the system temperature drop leads to a decrease in the hydrogen desorption, it is necessary to compensate for the temperature of the system. In this project, heat pipes are used to transfer the generated
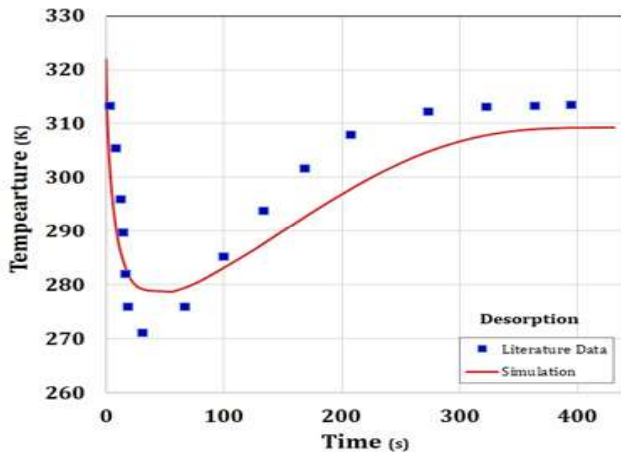
Fig. 5. Temperature changes over time during the desorption operation and compared with literature data [22].

heat from the cathode channel (due to the reaction of hydrogen with oxygen) to the hydride reservoir during the desorption operation. Thus, according to the results of Fig. 5, the temperature of the system starts to increase at about 30 seconds, and continues until the temperature reaches an equilibrium value (equivalent to the heat transfer rate by the heat pipe). The sudden drop in system temperature is due to the high mass transfer driving force (the difference in the hydrogen concentration in the solid phase and the gas phase) in the initial state of the operation. The initial steep slope of desorption of hydrogen results in a sudden decrease in the temperature of the system, despite the heat supply from the heat pipes. Subsequently, over time, with the reduction of the mass transfer driving force and the reduction of the energy consumption (due to the endothermic desorption process) heat transfer of the heat pipes can replace the energy consumption of the system. In addition, this figure represents a good agreement between literature data [22] and simulation results. The different between simulation and literature data can be due to the model assumptions. For example, we assume that enthalpy and entropy are constant and not a function of temperature. Gas is also assumed to be ideal. The error can be obtained from the following relation:

ADD (%) =

$$\sum \frac{|\text{experimental value} - \text{simulation value}|}{N} \times 100 \qquad (25)$$

Considering N=18, ADD is 1.34%.

In Fig. 6, the effect of the initial pressure of the adsorption tank on the amount of adsorbed hydrogen for the studied system in this project is shown. Similar to the results of Fig. 3, the adsorption rate of the hydrogen onto the metal powder is increasing over time.
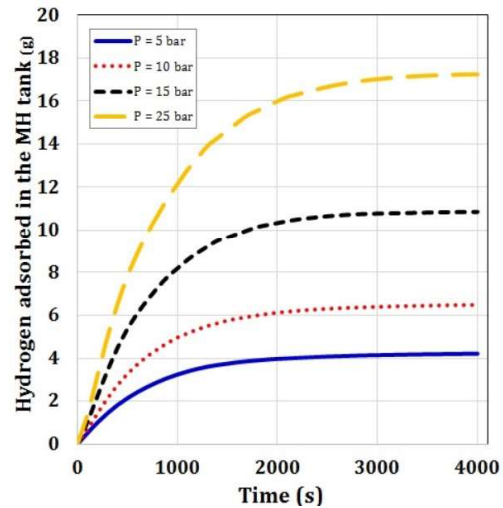

Fig. 6. Effect of initial pressure of the adsorption tank on the adsorbed hydrogen.

This figure shows the final amount of adsorbed hydrogen increases with the escalation of initial pressure of the reservoir. The final adsorbed hydrogen for the pressure of 5bar, 10, 15and 25 bar is 4.21, 6.48, 10.86 and 17.24 g, respectively. In other words, as the pressure increases from 5bar to 25 bar, the amount of hydrogen adsorption increases as much as 13.02 g. The adsorption of hydrogen molecules on the active sites of metal powder is a direct function of the partial pressure of hydrogen. Obviously, as the pressure increases the intermolecular interactions of the adsorbent (hydrogen) and the adsorbent (metal powder) increases and eventually leads to an increase in the formation of intermolecular bonds. Fig. 7 shows the amount of hydrogen in the hydride reservoir during the desorption operation in terms of time at the various initial pressures. This figure shows that over a period of 4000 seconds, the hydrogen content of the tank decreases from the initial values of 4.05, 6.3, 8.04, 16.2 g to the final values of 0.12, 0.9, 1.77, and 6.1 g correspond to the pressures of

5, 10, 15, and 25 bar, respectively. In other words, the amount of desorbed H2 will rise with the initial pressure to the amounts of 3.93, 5.39, 6.27, and 10.09 g corresponding to the pressures of 5, 10, 15, and 25 bar, respectively.
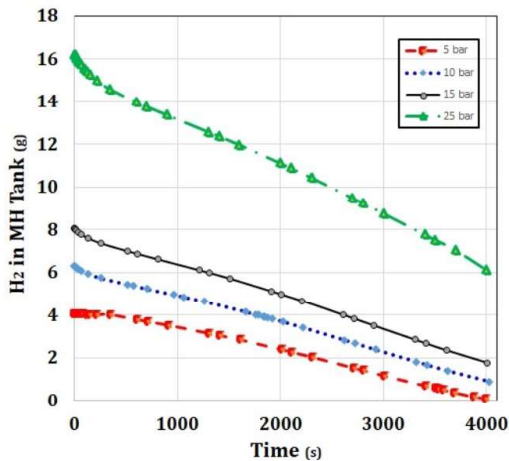

Fig. 7. Hydrogen amount in the tank over time during desorption operation at various initial pressures of the desorption operation (four heat pipes in use).

In other words, at the end of the desorption stage (4000 s), 5.39 g of hydrogen is purged from the hydride reservoir. At this stage, as the mass transfer driving force reduces over time, the efficiency of purging system is expected to decrease. It is worth noting that due to increased activation energy levels at each pressure, the amounts of hydrogen adsorbed and desorbed are not equal. After the formation of intermolecular bonds of hydrogen and metal each time, part of these bonds can no longer be broken at the desorption stage. Also, the number of unbroken intermolecular bonds increases in each cycle of adsorption and desorption. As the results of Figs. 6 and 7 show, the amount of desorbed hydrogen (5.39 g) is less than the adsorbed hydrogen content (6.48 g). Fig. 8 depicts the effect of the cooling water input temperature on the amount of adsorbed hydrogen and the temperature of the hydride reservoir. In the simulation conditions, the cooling water inlet temperature is investigated between 282 K and 323 K. As can be seen in this figure, the temperature of the cooling water first increases from 282 to 303 K resulting in an increase in the adsorbed hydrogen
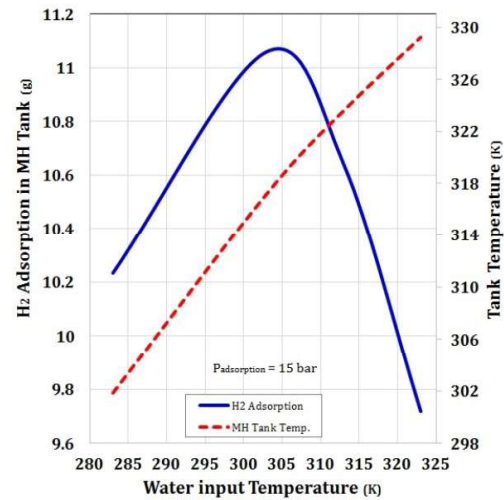

Fig. 8. Effect of cooling water input temperature on the amount of hydrogen adsorbed and tank temperature.

up to 0.83 g, and then as the temperature increases further, the amount of adsorbed hydrogen is reduced. Although the adsorption process is an exothermic operation and should keep the system temperature down to a reasonable level, it is important to control the temperature of the system so that it does not fall below a certain limit, which would have a negative effect on the diffusion coefficient of hydrogen. The results show that at temperatures below 303 K, the diffusion of hydrogen into the porous metal bulk pore decreases; therefore, the amount of adsorbed hydrogen is expected to decrease. On the other hand, if the system temperature is higher than 303 K, the amount of desired heat that should be removed from the system is reduced, which reduces the efficiency of hydrogen adsorption operations. In addition, the results of this figure clearly show that the temperature of the hydride reservoir increases almost linearly with the cooling water inlet temperature.

Figs. 9 to 11 show the temperature profiles of the various parts of the system in this study. Fig. 9 shows the temperature profile for heat pipes at 30 and 600s. As can be seen in Fig. 9, the MH tank temperature change is steep in the first 30s of adsorption due to the endothermic nature of adsorption. But at the end of the adsorption step (600s), the MH tank temperature changes in a small range (about 6K) because of the heat compensation required for adsorption by the heat pipes.
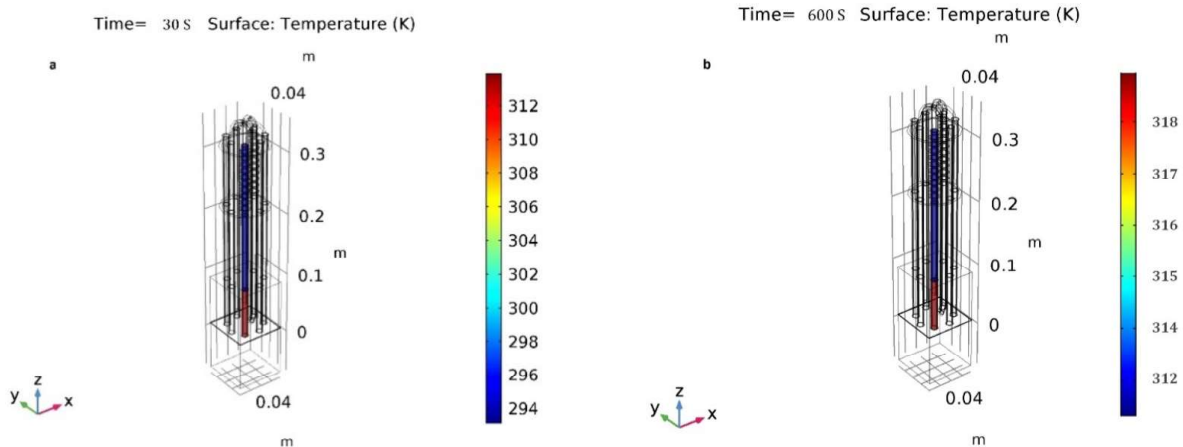
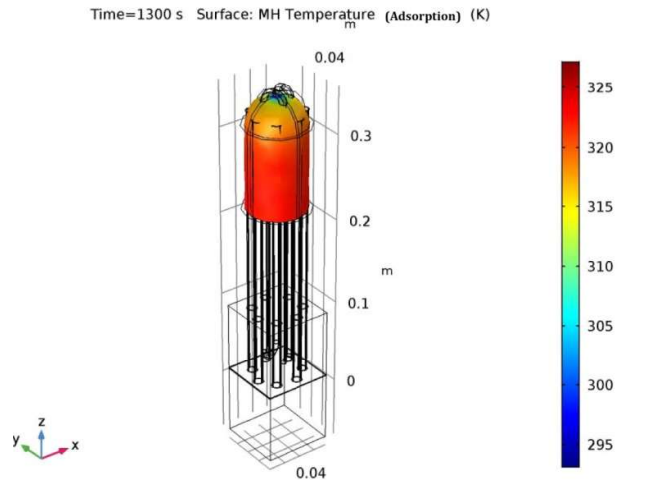**Fig. 9. Heat pipe temperature profile**

Fig. 10. Temperature profile of the MH tank (adsorption step)

Fig. 10 shows the uniformity of the hydride reservoir temperature during the adsorption stage. Since the cooling water flow helps to dispose of the heat generated by the process during adsorption operation, it is expected that the reservoir temperature will be uniform at this stage. According to this figure, the farther away from the hydrogen gas inlet, the higher the temperature; this is due to the increase in the released heat of the geometric volume (the inlet section is conical and the diameter is smaller than the other sections of the reservoir). Fig. 11 shows that the hydride reservoir temperature changes up to 5 K during desorption operations. Energy consumption due to the desorption operation as well as energy compensation through the heat pipes causes a temperature changes of up to maximum 5 K in different parts of the reservoir. Also, this figure

shows that the MH temperature increases with the number of heat pipes used in the operation.

As can be seen in Fig. 12, the discharge H_2 rate of MH is affected by its temperature. Both the H_2 flow rate and heat demand curves showed an almost similar value when using different numbers of heat pipes in the first thermal mode of the MH tank (Figs. 12a and 12c). In the first 515s of the desorption operation, when the initially released H_2 flows to the fuel cell, both hydrogen flow rate and heat in the MH tank reduce until the heat generated in the fuel cell is transferred to the MH tank by the heat pipes. Subsequently, the decreasing trend of tank temperature will stop at 297, 293, 295, 296.5 K corresponded to the use of one, two, three and four heat pipes, respectively (515 sec.). After that, the H_2 flow rate and heat demanded by the MH tank is affected by the performance of the
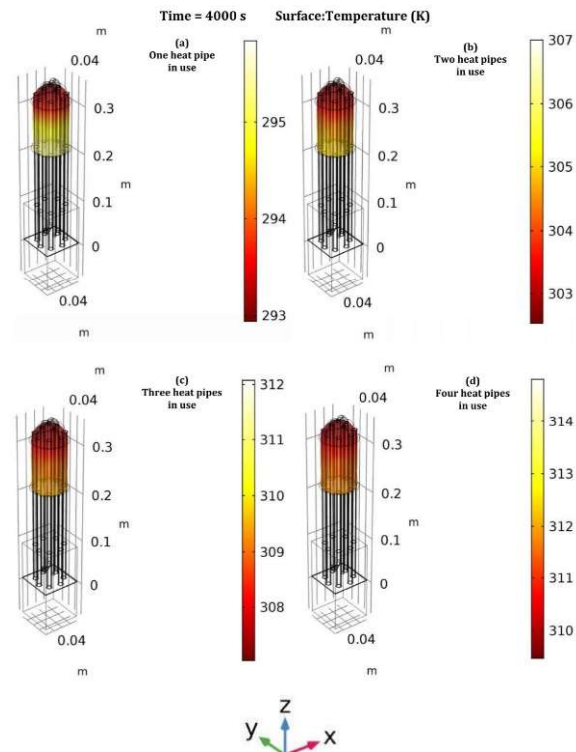
Fig. 11. Temperature profiles of MH tank Vs number of heat pipes in use (Desorption step).
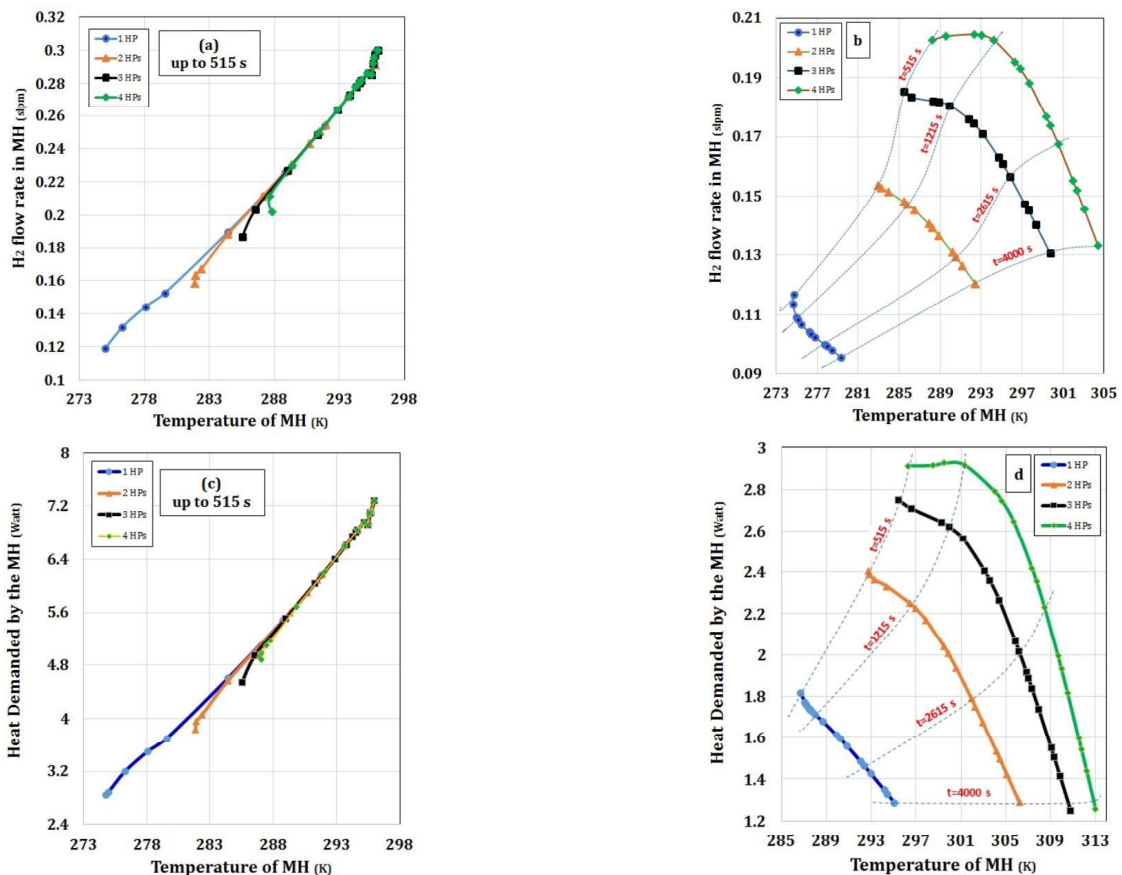

Fig. 12. Hydrogen flow rate and heat demanded for H$_2$ desorption as a function of MH temperature when coupled with a 25 W PEMFC for various numbers of heat pipes in use. a) and c) first 515s of the desorption step, b) and d) after 515s of the process.

number of heat pipes (second thermal mode of the MH tank). As can be seen in Fig. 12b, at any certain time of operation, the H_2 flow rate will be higher when number of heat pipes in use is larger. According to this figure, when four heat pipes are used, the H_2 flows through the MH tank up to 4100s when the flow rate falls to 0.05 slpm at the MH temperature of 313 K. By referring to the results of this figure, the maximum H_2 flow rate with four heat pipes is 0.121 slpm at 515s compared to the others H_2 flow rates of 0.113, 0.0995, and 0.0757 for three, two, and one heat pipes, respectively. Fig. 12d shows the heat demanded by the MH tank as a function of the number of heat pipes. At any given time of operation, the heat demanded by the MH tank is higher as the number of heat pipes used in the operation increases. As previously mentioned, the temperature of the MH increases as a result of the heat transferred from the fuel cell through the heat pipes. With respect to the results of this figure, from the given heat produced in the fuel cell, the heat power of one heat pipe is 1.8 W, but the heat transferred by the heat pipes reduces when the number of heat pipes used is more than one. Fig. 13 shows the hydrogen flow rate as a function of heat generation of the 25 W PEMFC and the heat demanded by the MH tank. According to this figure, the total hydrogen discharge rate of 0.304 slpm is achieved by only consuming 7.36 W of a total of 23.43 W of generated heat in the fuel cell. In this study, the maximum hydrogen discharge rate of 0.304 slpm coincided with 7.36 W of a total of 23.48 W generated heat in the fuel cell. Note that, with reference to Figs. 12a and 12c, the maximum discharge rate of H_2 is independent of the number of heat pipes because this maximum was achieved in the first 515s of the desorption operation. Also, this figure indicates that it is necessary to recharge the hydrogen storage tank if the H_2 flow rate falls to 0.18 slpm because the heat generation curve is then located under the heat demanded values and therefore the fuel cell cannot supply enough heat for H_2 desorption. In Fig. 14, the hydrogen flow rate in the desorption stage is simulated when MH storage is coupled to a 500 W PEMFC. As can be seen in this figure, the
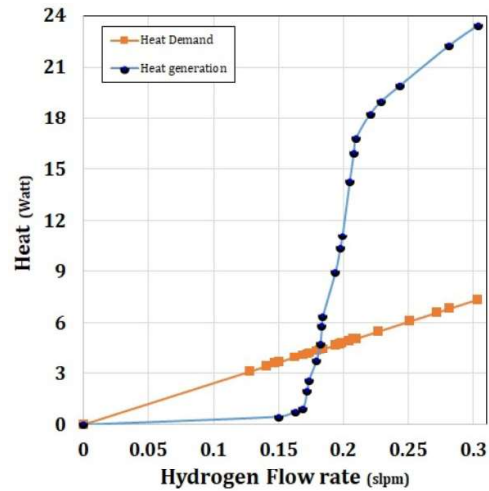

Fig. 13. Hydrogen flow rate as a function of heat generation for the 25 W PEMFC and the heat demanded by the MH tank at various initial pressures of the desorption operation.

proposed model geometry improves the release rate of hydrogen up to 45 % compared to the same fully system (system described in [5]). In fact, this model of this work raised the maximum H_2 flow rate from 3.70 slpm to 5.37 slpm.
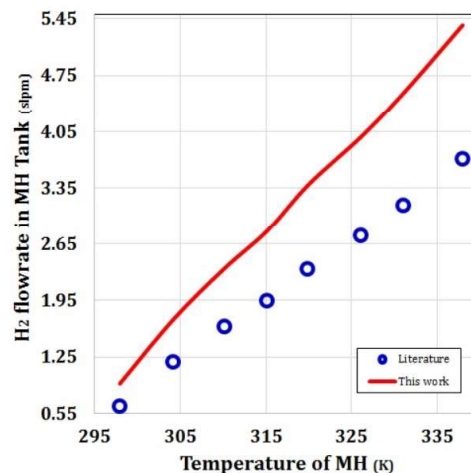

Fig. 14. Desorption flow rate of hydrogen vs. MH temperature when coupled with a 500 W PEMFC (four heat pipes in use) as compared with the literature data. [5].

4. Conclusions

In this work, a modelling study of thermal coupling of a PEMFC with a MH tank was carried out. The thermal coupling was carried out using heat pipes, in which the heat released in the cathode channel of the fuel

cell is directed to the MH storage causing hydrogen to be released at a higher rate. The simulation of the designed system was performed using CFD. The system was designed in two stages. In the first stage, hydrogen is adsorbed in the hydride reservoir, then in the second stage, part of this hydrogen is released for use in a PEMFC. For this purpose, the metal powder in the storage tank was assumed to be $LaNi_5$. Simulation results indicated that the MH temperature increased from 293.15 K to approximately 335.15 K in the first 80 seconds of the adsorption stage, then the reservoir temperature decreased to nearly the initial temperature. In the first 30 seconds of the desorption stage, the MH temperature decreased from 323.15 to 278.15 K, then the heat pipes compensated for the temperature of the system leading to an increase in the temperature of the desorption reservoir up to 31 K. In the other words, using heat pipes helps to reduce the temperature difference for longer than 30 seconds. Furthermore, the final amount of adsorbed hydrogen increases with the escalation of the initial pressure of the MH tank. The final adsorbed hydrogen for the pressures of 5, 10, 15 and 25bar is 4.21, 6.48, 10.86, and 17.24 g, respectively. Moreover, the amount of desorbed H_2 increases with the initial pressure with the amount of 3.93, 5.39, 6.27, and 10.09 g corresponding to pressures of 5, 10, 15, and 25 bar, respectively. Additionally, H_2 adsorption performance is improved at the cooling temperature of 303 K. Both the H2 flow rate and the heat demanded by the MH tank are higher when a number of heat pipes are in use. Simulation results show that both hydrogen flow rate and heat demanded in the MH tank are reduced in the first 515s of desorption operation, and the maximum H_2 flow rate of 0.203 slpm is obtained with four heat pipes compared to H_2 flow rates of 0.185, 0.153, and 0.117 for three, two, and one heat pipes used, respectively. In addition, results show that one heat pipe has 1.8 W heat power, but this heat power could be reduced when multiple heat pipes were used as shown by a given heat produced in the fuel cell. The maximum hydrogen discharge rate of 0.304 slpm was achieved at the expense of 7.36 W from a total of 23.43 W generated heat in

the fuel cell. Furthermore, the mesh independency test showed the obtained results for the normal and fine size mesh are almost the same. Thus, normal size mesh can be used instead of fine mesh to increase the computational speed. Moreover, based on the simulation results, the presented geometry improves the release rate of hydrogen by 45% compared to the same fully system (compared to the system described in [5]).

Nomenclature

C_p	Gas heat capacity (j/kg.K)
C_a	Adsorption constatnt
C_d	Desorption constant
D_{ij}	Binary diffusion coefficient (m^2/s)
D_{ik}	Knudsen diffusion coefficient of ith component (m^2/s)
$D_{e,ik}$	The mass diffusion coefficient of component i^{th} (m^2/s)
d	Thickness of thin film (m)
d_k	Gas and liquid phase concentration difference parameter (--)
h	Heat transfer coefficient ($W.m^2$.k)
J_i	Mass flux of ith component in the gas phase (kg/m^2.s)
k_f	Reaction kinetic constant of forward reaction (1/s)
k_r	Reaction kinetic constant of revers reaction (1/s)
k	Gas conductivity coefficient (j/kg.K)
k_{disp}	Dispersed heat conduction coefficient (j/kg.K)
k_{eff}	Effective heat transfer coefficient (W/m^2.K)
k_p	Particle conductivity coefficient (j/kg.K)
M	Molecular weight (kg/kmol)
M_k	Molecular weight of ith component (kg/kmol)
M_n	Total molecular weight (kg/kmol)
P	Pressure (Pa)
Q	Heat source (W/m^3)
q	Heat flux (W/m^2)
Q_p	Pressure work (W/m^3)
Q_{vd}	Viscous dissipation (W/m^3)
Ri	Reaction of ith component in the gas phase (kg/m^2.s)

r   Reaction rate (mol/kgcat.K)

T   Temperature (K)

t   Time (s)

U   Gas velocity (m/s)

w_i Weight fraction of ith component in the gas phase (--)

x_k Mass fraction of ith component in the solid phase (--)

Greek symbols

β Velocity gradient at the surface (s-1)

ε Void fraction of the MH tank (gas phase) (--)

θ Void fraction of metal powder (solid phase) (--)

μ Viscosity (Pa.s)

ν Stoichiometric coefficient of ith component in reaction (--)

ρ Density (kg/m^3)

τ_F Electrode tortuosity (--)

References

[1] Alapati, S.V., J.K. Johnson, and D.S. Sholl, "Predicting reaction equilibria for destabilized metal hydride decomposition reactions for reversible hydrogen storage", The Journal of Physical Chemistry C, 2007, 111(4): 1584.

[2] Gadre SA, Ebner AD, Al-Muhtaseb SA, Ritter JA. "Practical modeling of metal hydride hydrogen storage systems", Industrial & engineering chemistry research. 2003, 42(8):1713.

[3] Liu C, Chen Y, Wu C-Z, Xu S-T, Cheng H-M. "Hydrogen storage in carbon nanotubes revisited", Carbon. 2010, 48(2):452.

[4] Westman M, Chun J, Choi YJ, Rönnebro EC. "Materials Engineering and Scale-up of Fluid Phase Chemical Hydrogen Storage for Automotive Applications", Energy & Fuels. 2015, 30(1):560.

[5] Tetuko AP, Shabani B, Andrews J. "Thermal coupling of PEM fuel cell and metal hydride hydrogen storage using

heat pipes", international journal of hydrogen energy. 2016, 41(7): 4264.

[6] Shabani B, Andrews J, Watkins S. "Energy and cost analysis of a solar-hydrogen combined heat and power system for remote power supply using a computer simulation", Solar Energy. 2010, 84(1): 144.

[7] Shabani B, Andrews J. "An experimental investigation of a PEM fuel cell to supply both heat and power in a solar-hydrogen RAPS system", International journal of hydrogen energy. 2011, 36(9): 5442.

[8] Oriňáková R, Oriňák A. "Recent applications of carbon nanotubes in hydrogen production and storage", Fuel. 2011, 90(11): 3123.

[9] Burke KA, Jakupca I. Unitized regenerative fuel cell system gas storage/radiator development. SAE transactions. 2004,1807.

[10] Silva AP, Galante RM, Pelizza PR, Bazzo E." A combined capillary cooling system for fuel cells", Applied Thermal Engineering. 2012, 41:104.

[11] Faghri., 1st ed., A Heat pipe science and technology, Taylor & Francis, 1995.

[12] Førde T, Eriksen J, Pettersen A, Vie P, Ulleberg Ø. "Thermal integration of a metal hydride storage unit and a PEM fuel cell stack", international journal of hydrogen energy. 2009, 34(16):6730.

[13] Wang H, Prasad AK, Advani SG. "Accelerating hydrogen absorption in a metal hydride storage tank by physical mixing", International Journal of Hydrogen Energy. 2014, 39(21):11035.

[14] Wu Z, Yang F, Zhu L, Feng P, Zhang Z, Wang Y. "Improvement in hydrogen desorption performances of magnesium based metal hydride reactor by incorporating helical coil heat exchanger", International Journal of Hydrogen Energy. 2016, 41(36):16108.

[15] Mellouli S, Askri F, Dhaou H, Jemni A, Nasrallah SB. "A study of the thermal behavior of a deformable metal-hydride bed", International Journal of Hydrogen Energy. 2016, 41(3):1711.

[16] Saleh IM, Rashid A, Zhang H."Simplified mathematical model of proton exchange membrane fuel cell based on horizon fuel cell stack", Journal of Modern Power Systems and Clean Energy. 2016, 4(4):668.

[17] Pan C, Zhou Y, Wang J. CFD study of heat transfer for oscillating flow in helically coiled tube heat-exchanger. Computers & Chemical Engineering. 2014, 69:59.

[18] Pfeifer P, Wall C, Jensen O, Hahn H, Fichtner M. "Thermal coupling of a high temperature PEM fuel cell with a complex hydride tank", international journal of hydrogen energy. 2009, 34(8):3457.

[19] Pooyoo N, Kumar S, Charoensuk J, Suksangpanomrung A. "Numerical simulation of cylindrical heat pipe considering non-Darcian transport for liquid flow inside wick and mass flow rate at liquid–vapor interface", International journal of heat and mass transfer. 2014, 70:965.

[20] Busqué Somacarrera, Raquel. Metal hydride state of charge estimator. Development and experimental validation of the hydrogen storage system model. BS thesis. Universitat Politècnica de Catalunya, 2015.

[21] Mellouli S, Abhilash E, Askri F, Nasrallah SB. "Integration of thermal energy storage unit in a metal hydride hydrogen storage tank", Applied Thermal Engineering. 2016, 102:1185.

[22] Chibani A, Bougriou C. "Effect of the tank geometry on the storage and destocking of hydrogen on metal hydride ($LaNi_5H_2$)", International Journal of Hydrogen Energy. 2017, 42(36):23035.

[23] Santhanam S, Schilt C, Turker B, Woudstra T, Aravind P. "Thermodynamic modeling and evaluation of high efficiency heat pipe integrated biomass Gasifier–Solid Oxide Fuel Cells–Gas Turbine systems", Energy. 2016, 109:751.